Eur J Nutr (2013) 52:749–758
DOI 10.1007/s00394-012-0381-x

ORIGINAL CONTRIBUTION

Evidence of altered biochemical composition in the hearts of adult intrauterine growth-restricted rats

Vladislava Zohdi · Bayden R. Wood · James T. Pearson · Keith R. Bambery · M. Jane Black

Received: 4 March 2012 / Accepted: 10 May 2012 / Published online: 29 May 2012

Abstract
Purpose Epidemiological studies clearly link intrauterine growth restriction with increased risk of cardiac disease in adulthood. The mechanisms leading to this increased risk are poorly understood; remodeling of the myocardium is implicated. The aim was to determine the effect of early life growth restriction on the biochemical composition of the left ventricular myocardium in adult rats.
Methods Wistar Kyoto dams were fed either a low protein diet (LPD; 8.7 % casein) or normal protein diet (NPD; 20 % casein) during pregnancy and lactation; from weaning, the offspring were fed normal rat chow. At 18 weeks of age, the biochemical composition of the hearts of NPD control ($n = 9$) and LPD intrauterine growth-restricted ($n = 7$) offspring was analyzed using Fourier Transform Infrared (FTIR) micro-spectroscopy.
Results Body weights at postnatal day 4 were significantly lower and remained lower throughout the experimental period in the LPD offspring compared to controls. FTIR analysis of the infrared absorption spectra across the whole "fingerprint" region (1,800–950 cm^{-1}) demonstrated wider variation in absorbance intensity in the LPD group compared to controls. In particular, there were marked differences detected in the protein (1,540 cm^{-1}), lipid (1,455 and 1,388 cm^{-1}), proteoglycan (1,228 cm^{-1}) and carbohydrate (1,038 cm^{-1}) bands, indicating increased lipid, proteoglycan and carbohydrate content in the growth-restricted myocardium.
Conclusion In conclusion, changes in the biochemical composition of the myocardium provide a likely mechanism for the increased vulnerability to cardiovascular disease in offspring that were growth restricted in early life.

Keywords Early life growth restriction · Fourier transform infrared (FTIR) micro-spectroscopy · Cardiac remodeling · Fetal programming

Keith R. Bambery, M. Jane Black: Joint senior authors.

V. Zohdi · M. J. Black (✉)
Department of Anatomy and Developmental Biology, Monash University, Wellington Rd, Clayton, VIC 3800, Australia
e-mail: Jane.black@monash.edu.au; jane.black@monash.edu

B. R. Wood · K. R. Bambery
Centre for Biospectroscopy and School of Chemistry, Monash University, Clayton, VIC 3800, Australia

J. T. Pearson
Monash Biomedical Imaging, Monash University, Clayton, VIC 3800, Australia

J. T. Pearson
Department of Physiology, Monash University, Clayton, VIC 3800, Australia

Introduction

The etiology of cardiovascular disease is directly influenced by both genetic and lifestyle factors, and it is now well recognized that the very early prenatal environment can program the heart for susceptibility to cardiovascular disease later in life; intrauterine growth-restricted (IUGR) infants are particularly vulnerable. Up to fifteen percent of all pregnancies worldwide exhibit some degree of intrauterine growth restriction (IUGR) [1]; it is multifactorial in origin and can be caused by factors such as placental insufficiency, maternal infections, hypoxia and dietary undernutrition and/or malnutrition [2–5].

Both clinical and experimental studies demonstrate a strong link between IUGR and adverse cardiovascular consequences in adulthood [2, 5]. For instance,

epidemiological studies from many populations worldwide have reported an increased incidence of ischemic heart disease in adulthood in subjects that were born of low birth weight [6, 7]. Importantly, in this regard, the USA Nurses' Health Study in which the health of 121,700 women were followed from 1976 clearly showed that these strong associations between low birth weight and heart disease remain even after adjustments for adult smoking, physical activity, dietary habits and socio-economic status [8]. Also of concern, in a recent study, cardiac function was shown to already be impaired in IUGR children by 5 years of age; these children also exhibited elevated blood pressure [9]. In accordance with the human findings, in rodent models, IUGR offspring have been shown to be more vulnerable to the development of hypertension, cardiac fibrosis, cardiac dysfunction and to myocardial ischemia–reperfusion injury in adulthood [10–13]; also alterations in genes regulating myocardial glucose metabolism have been reported [14].

In order to develop strategies to prevent the increased incidence of ischemic heart disease in subjects that were growth restricted in early life, it is imperative to gain an understanding of the mechanisms underlying this relationship. In this regard, changes in the extracellular matrix are a likely cause. The myocardial extracellular matrix is a complex three-dimensional network including collagens, elastin, proteoglycans and glycoproteins [15]. Many complex factors contribute to decreased cardiac performance. Extracellular matrix remodeling is thought to play an important role in this process [16]. We therefore propose that IUGR leads to alterations in the biochemical structure of the heart which would have the potential to ultimately lead to impaired electrical conductivity and contractility of the myocardium. In this study, we have begun to address this hypothesis by examining, using Fourier transform infrared (FTIR) micro-spectroscopy, whether there are differences in the molecular structure and biochemistry of the myocardium in adult rats that were either appropriately grown or growth restricted in early life.

FTIR spectroscopy is a powerful technique that has been successfully applied to many biomedical research applications including analyses of cardiac tissue. We have recently performed 3D FTIR imaging on the mouse heart and showed how protein distribution varies within the myocardium [17] and others have examined biochemical differences in the myocardium in the presence of diabetes and following myocardial infarction [18–20]. This technique allows assessment of the spatial distribution of extracellular molecules as well as quantitative assessment of their tissue levels. FTIR spectra record the transitions in vibrational modes of molecular functional groups as a result of absorption of mid-infrared photons. Consequently, FTIR spectra of tissues are representative of their constituent biomolecules such as proteins, lipids, carbohydrates and nucleic acids. From the relative intensities of absorbance bands, associated with various functional groups, the relative content of the different biomolecules present in the sample can be obtained. FTIR micro-spectrometers may be coupled to a focal plane array (FPA) or linear array detector to enable rapid acquisition of thousands of spectra as a hyper spectral data image. Each spectrum can be correlated to a particular x–y coordinate and thus enables imaging of the molecular and structural composition directly within the tissue.

Experimental methods

Animals and diet treatment

Ten-week-old female and male Wistar Kyoto (WKY) breeder rats were obtained from the Australian Resource Centre, Perth, Australia. Female breeders were placed on either a low protein diet (LPD; 8.7 % casein and 15.6 MJ/kg) or normal protein diet (NPD; 20 % casein and 16.1 MJ/kg) [21] 2 weeks prior to pregnancy (to allow them to adapt to the diet), during pregnancy and 2 weeks after birth (diets were commercially available from Specialty Feeds, Glen Forrest, Perth, Western Australia). After this time, all dams were fed standard rat chow. Female breeders were housed individually and maintained on a 12:12-h light–dark cycle and at a constant temperature of 21 ± 1 °C. Food and water were provided ad libitum. At birth, the litters were reduced to eight pups and the female offspring allowed to grow to adulthood (NPD: $n = 9$; LPD: $n = 7$). There was no difference in litter size between groups, and the male/female ratio was not different between NPD and LPD litters. Only female offspring were examined in this study as we have recently shown increased vulnerability to cardiac dysfunction in adulthood in the female offspring in this model [22]; one female offspring from each litter was used. Body weight of the offspring was measured daily from day 4 until weaning (4 weeks of age), then once a week until the experimental endpoint (18 weeks of age). After weaning all offspring were fed standard rat chow.

Animal care and experimental procedures were carried out in accordance with the National Health and Medical Research Council (NH&MRC) of Australia "Code of Practice for the Care and Use of Animals for Scientific Purposes" and were approved by the Monash University, School of Biomedical Sciences Animal Ethics Committee A.

Organ collection and tissue processing

At 18 weeks of age, the rats were anesthetized and perfusion-fixed retrogradely (via a catheter in the abdominal

aorta) with 4% formaldehyde at a constant pressure of 100 mmHg [23]. Prior to perfusion-fixation heparin sodium (to prevent blood from clotting), papaverine hydrochloride (to maximally dilate the vasculature) and potassium chloride (to arrest the hearts in diastole) were administered via the abdominal catheter. The fixed hearts were excised, trimmed of fat and connective tissue and weighed. The atria were excised from the hearts, and the right and left ventricles with adjoining interventricular septum were cut into 1-mm-thick transverse slices using a razor blade cutting device.

Heart wall volume determination

An orthogonal grid was superimposed over the ventricular slices and the volume of the right ventricular (RV) wall and left ventricular (LV) wall and adjoining septum (LV + S) were determined using the Cavalieri principle [24].

Quantification of cardiac fibrosis

Every second LV slice was embedded in paraffin, sectioned at 5-μm-thickness and stained with picrosirius red [21]. To measure interstitial fibrosis, the sections were uniformly, systematically sampled, and the percentage of collagen within the interstitium was quantified using image analysis (Image Pro Plus Version 6.0, Media Cybernetics) [21].

FTIR micro-spectroscopy: sample preparation and data acquisition

Alternate ventricular slices were used for FTIR scanning. Paraffin blocks were sectioned at 4 μm using a microtome (Micro Tec, Type 4060 Germany) and mounted on FTIR-reflective slides (Kevley Technologies). The slides were dewaxed (three washes in clean xylene) prior to FTIR imaging. Spectra were collected with a Varian "Stingray"system that combines a 7000 series rapid-scan spectrometer containing a Michelson interferometer, a 600 UMA microscope and a liquid nitrogen cooled mercury–cadmium–telluride 64 × 64 pixel FPA detector. FTIR spectral data images were recorded in the range 1,800–800 cm^{-1} at 6 cm^{-1} resolution. For each tissue section, two sets of images were obtained. The first set of images covered areas of 0.7 mm × 0.7 mm that included only LV free wall with a spatial resolution of 11 μm per pixel (4 pixel aggregation and 64 co-added interferograms). The second set of images comprised the whole LV (that is the interventricular septum, free wall and papillary muscles) with spatial resolution of 176 μm per pixel (1,024 pixel aggregation and 8 co-added scans). Background spectra were collected from a clean region on the FTIR-reflective slide. A visible light image of the sample was also collected. The total data acquisition times for each image of LV free wall and the whole LV were approximately 1 min and 9 h, respectively.

Unsupervised hierarchical cluster (UHC) analysis

To analyze the spectral data sets, we used unsupervised hierarchical cluster (UHC) analysis that enables analysis of the similarity of spectra in a data set by well-established algebraic methods and assigns 'cluster membership' based on this similarity [25]. The pseudo-color maps, based on the spectral similarity only, do not require any prior knowledge about the type of tissue, state of disease or composition. Hence, this analysis is referred to as an 'unsupervised' method [25].

Statistical analysis

Body weights at 4 days of age, morphometric data and levels of cardiac fibrosis at 18 weeks of age were analyzed with a Student's t test. Body weight over time was analyzed using a repeated measure of two-way analysis of variance (ANOVA). Statistical significance was accepted at $P \leq 0.05$.

Chemical images were generated using Varian Resolutions Pro software. Figure 1 displays an example of a typical FTIR spectrum from the LV free wall showing the major band positions and the integrated areas under the bands used to produce the FTIR chemical images. Assignments of band vibrations are given in Table 1. The area under the amide II band at ~1,540 cm^{-1} is representative of the total protein content. Analysis of the dominant amide I band (1,650 cm^{-1}) from proteins was not included due to dispersion effects in the heart tissue as evidenced by the apparent shifting about of the amide I band center in the range 1,643–1,653 cm^{-1} and the variation in the ratio of the amide I to amide II band intensities. It has recently been demonstrated that these dispersion effects are principally due to resonant Mie scattering and while it is normally most prominent on the amide I band, it is not confined to the amide I band and may influence any band in the spectrum [26]. The area under the pair of bands at 1,455 and 1,388 cm^{-1} is indicative of the lipid content in the tissue [27, 28]. The band at 1,228 cm^{-1} (labeled "mixed" band) arises from several contributing functional groups; (a) the protein amide III mode, (b) the asymmetric phosphate stretching vibration from nucleic acids, phospholipids and phosphorylated proteins and (c) the sulfate symmetric stretch from proteoglycans. The band at 1,038 cm^{-1} is assigned to carbohydrates [27, 28].

The average spectrum from each animal was calculated in Cytospec (www.cytospec.com) from spectra in the FTIR image that passed quality tests for signal-to-noise ratio and

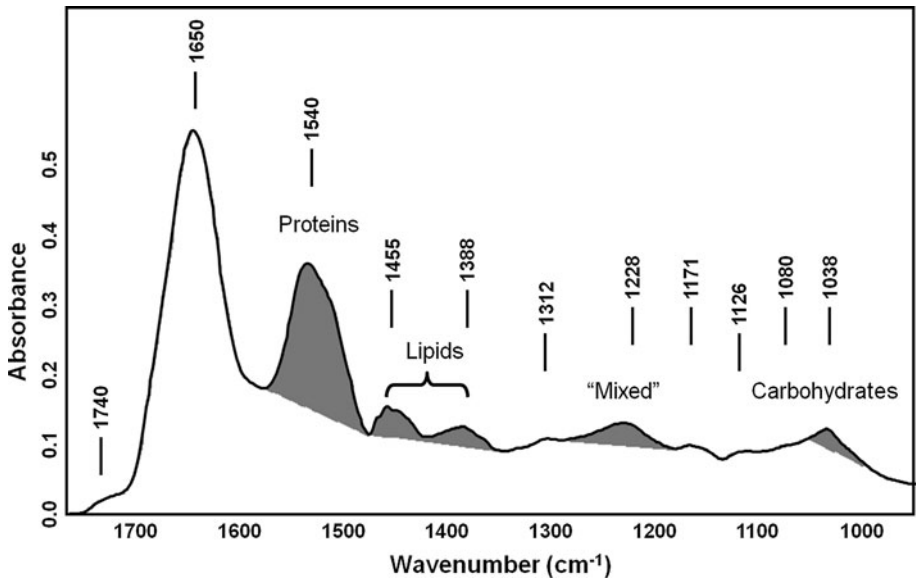

Fig. 1 Typical FTIR spectra of the left ventricle (LV). *Gray* areas indicate the integrated areas used to produce the chemical images in Figs. 5 and 6. Proteins (1,583–1,477 cm^{-1}), lipids (1,477–1,350 cm^{-1}), "mixed" contribution band (1,295–1,186 cm^{-1}) and carbohydrates (1,060–1,000 cm^{-1})

Table 1 Band assignments of major absorptions in IR spectra of heart tissue in 1,800–950 cm^{-1} region

Frequency (cm^{-1})	Assignments
1,740	C=O stretching: ester functional groups in lipids [28]
1,650	Amide I: (mainly protein C=O stretching) [19]
1,540	Amide II: (protein N–H bending, C–N stretching) [19]
1,468	CH_2 scissoring: lipids [27, 28]
1,386	CH_3 bending: lipids [27, 28]
1,338	CH_2 side chain vibrations of collagen [18, 19]
1,312	Collagen (amide III) [18]
1,282	Collagen amide III vibration [18, 19]
1,228 region (1,235–1,246)	Sulfate stretch from proteoglycans [34–37] Collagen amide III vibration [18, 19, 32] PO_2^- asymmetric stretching: phospholipids, nucleic acids [19, 27]
1,201	Collagen (amide III) [18, 19, 32]
1,171	CO–O–C asymmetric stretching: ester bonds in cholesterol esters and phospholipids [47]
1,154	C–O stretching: glycogen, nucleic acids [48]
1,126	Glycogen [49]
1,080	PO_2^- symmetric stretching: phospholipids, nucleic acids [27] C–O stretching: glycogen, oligosaccharides, glycolipids [48], proteoglycans [36, 37]
1,038	C–O stretching vibrations of the carbohydrate residues [50] and present in proteoglycans [36]
994	Nucleic acids [51]
968	Nucleic acids [51]

IR infrared

dispersive line shape artifacts [29]. To produce the two group average spectra, the average spectrum from each animal was first vector normalized (mean-centered) to remove any possible bias from tissue section thickness variations. Second derivative spectra were calculated from the group average spectra using the Savitsky Golay algorithm (9 smoothing points). Second derivative analysis enables resolution of "hidden" band features in the spectra. Second derivative spectra were statistically analyzed using UHC analysis in Cytospec.

Results

Body weights, absolute and relative LV + S weights and wall volumes

The LPD offspring were significantly smaller at postnatal day 4 compared with NPD offspring (NPD: 7.19 ± 0.24 g and LPD: 6.16 ± 0.28 g; $P < 0.015$), and they remained significantly smaller over the experimental period ($P_{Diet} < 0.0001$; $P_{Time} < 0.0001$; two-way ANOVA). However, at 18 weeks of age when comparing the two groups, no differences in body weight were detected. At 18 weeks of age, there were no differences in absolute (NPD: 1,400 ± 43 mg and LPD: 1,382 ± 39 mg; $P > 0.81$) or relative (NPD: 5.5 ± 0.2 mg/g and LPD: 5.6 ± 0.2 mg/g; $P > 0.88$) heart weights. There were also no significant differences in the absolute LV + S weights and relative LV + S weights between the groups ($P > 0.88$ and $P > 0.68$, respectively; Table 2). Absolute LV + S wall volumes were significantly

Table 2 Absolute and relative LV + S weights and volumes of the rat offspring at 18 weeks of age

	NPD ($n = 9$)	LPD ($n = 7$)	P value
LV + S weight (mg)	830 ± 23	824 ± 24	0.88
LV + S weight: body weight (mg/g)	3.3 ± 0.1	3.4 ± 0.1	0.68
LV + S volume (mm^3)	742 ± 22	658 ± 17	0.01
LV + S volume: body weight (mm^3/g)	3.0 ± 0.1	2.7 ± 0.1	0.08

Data are mean ± standard error of the mean

LV + S left ventricle including interventricular septum

reduced in the LPD offspring compared to controls ($P < 0.01$; Table 2), but when adjusted to body weight, there was no difference between the groups ($P < 0.08$; Table 2).

Cardiac fibrosis

There was no significant difference ($P > 0.05$) in the amount of collagen deposition within the LV + S between NPD (4.49 ± 0.40 %) and LPD (5.11 ± 0.38 %) offspring at 18 weeks of age.

FTIR micro-spectroscopic analyses

Figure 2 shows the average FTIR spectra for each individual animal in the spectral region 1,800–950 cm^{-1} for the NPD group and LPD groups. In the spectral range 1,455–1,038 cm^{-1}, the LPD offspring (five of the seven animals studied) exhibited much stronger absorbance compared to the controls; the remaining two LPD offspring exhibited an absorbance similar to that of the NPD group. Hence, the LPD group showed a wider variation in absorbance intensity compared to controls (particularly in the region 1,477–950 cm^{-1}). Figure 3 shows distinct differences in the second derivative average spectra between the NPD offspring and LPD offspring across the spectral region 1,425–950 cm^{-1}. The band maxima in the original spectra become minima after calculating the second derivative. Bands at 1,038, 1,080, 1,126, 1,154, 1,171, 1,228, 1,312, 1,367 and 1,388 cm^{-1} were observed to be enhanced in the LPD offspring group compared to the control group. Importantly, the second derivative analysis revealed several unchanged band profiles between the LPD offspring and NPD offspring groups. These unchanged bands were found at 968, 994, 1,201, 1,282 and 1,338 cm^{-1}. The unchanged bands at 968 and 994 cm^{-1} were assigned to nucleic acids, and the 1,201, 1,282 and 1,338 cm^{-1} bands were assigned to collagen. Hence, indicating there was no change in nucleic acid content and collagen content between the two groups. UHC analysis distinguished the LPD versus the NPD offspring from the spectra in the range 1,800–950 cm^{-1} (Fig. 4). Cluster average second derivative spectra confirmed that protein, collagen and DNA content were not significantly changed between the two groups.

FTIR chemical images from the LV free wall and entire LV (LV + S) are shown in Figs. 5 and 6, respectively; (NPD images are shown in Figs. 5a–d, and 6a–d, respectively and LPD images shown in Figs. 5e–h and 6e–h, respectively). In Figs. 5 and 6, the columns (from left to right) depict FTIR chemical images based on the following spectral regions: proteins (amide II at 1,540 cm^{-1}), lipids (1,455 and 1,388 cm^{-1}), the "mixed" contributions band at 1,228 cm^{-1} and carbohydrates (1,038 cm^{-1}).

Protein bands: The NPD group (Figs. 5a, 6a) and LPD group (Figs. 5e, 6e) showed similar amide II absorbance in the LV free wall and in the whole LV as indicated by UHC analysis.

Lipid bands: Hearts from LPD offspring (Figs. 5f, 6f) exhibited a significantly higher lipid content compared to NPD controls (Fig. 5b, 6b) (apparent as increased red areas in the image). The distribution of lipids in the LV free wall (Fig. 5b) and whole LV (Fig. 6b) in the NPD group closely follows the pattern of protein content (Figs. 5a, 6a), thus indicating that the lipid content is spatially associated with the proteins. The same was found to be true for the distribution of proteins and lipids in the LV free wall and whole LV of the LPD offspring (Figs. 5e, f, 6e, f, respectively). The higher lipid content in the myocardium of the LPD group was also evidenced by the band at 1,740 cm^{-1} (assigned to ester functional groups in lipids) that had an increased intensity compared to the NPD group (Fig. 2).

Mixed contributions band at 1,228 cm^{-1}: The most striking difference in the biochemical composition of the LV myocardium was observed in the mixed contribution band. There was a marked increase in absorbance in the mixed contributions band at 1,228 cm^{-1}. FTIR micro-spectroscopic analysis revealed relatively low absorbance in the LV of the NPD offspring (Figs. 5c, 6c) and strong absorbance in the LPD offspring (Figs. 5g, 6g). As was found for the lipid images, the FTIR images based on the mixed contributions band exhibited a similar spatial distribution to the protein images (NPD: Figs. 5a, 6a, LPD: Figs. 5e, 6e).

Carbohydrate bands: Figs. 5d and 6d (NPD offspring) and Figs. 5h and 6h (LPD offspring) show the spatial intensity of carbohydrates within the LV free wall and whole LV, respectively. Some of the average spectra from the individual animals within the LPD offspring group exhibited the characteristic glycogen triplet of bands at 1,038, 1,080 and 1,126 cm^{-1}; that probably indicates variation in the stored glycogen content within LPD group. The individual animals within the NPD group all appeared

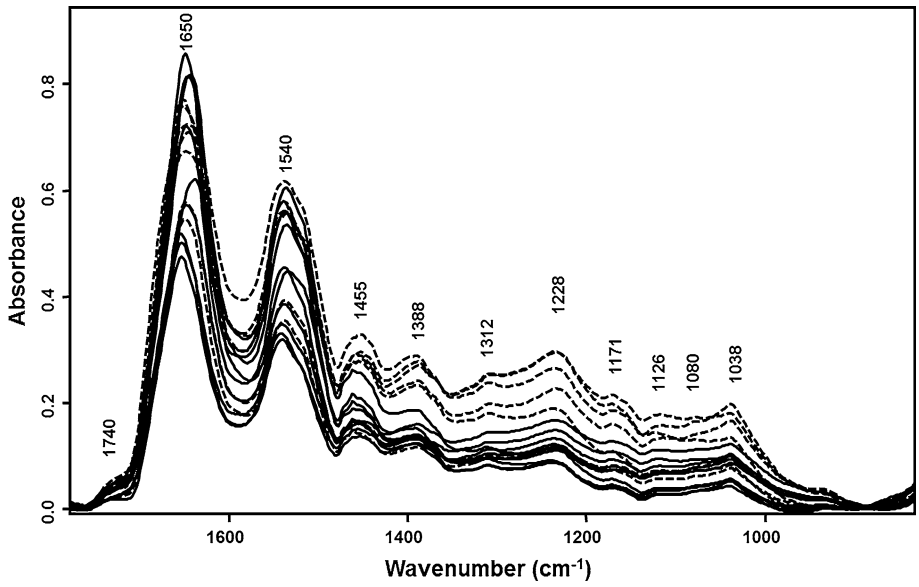

Fig. 2 Average spectra for individual animals in NPD (*solid line*, $n = 9$) and LPD (*dashed line*, $n = 7$) groups across 1,800–950 cm^{-1} spectral window from LV free wall

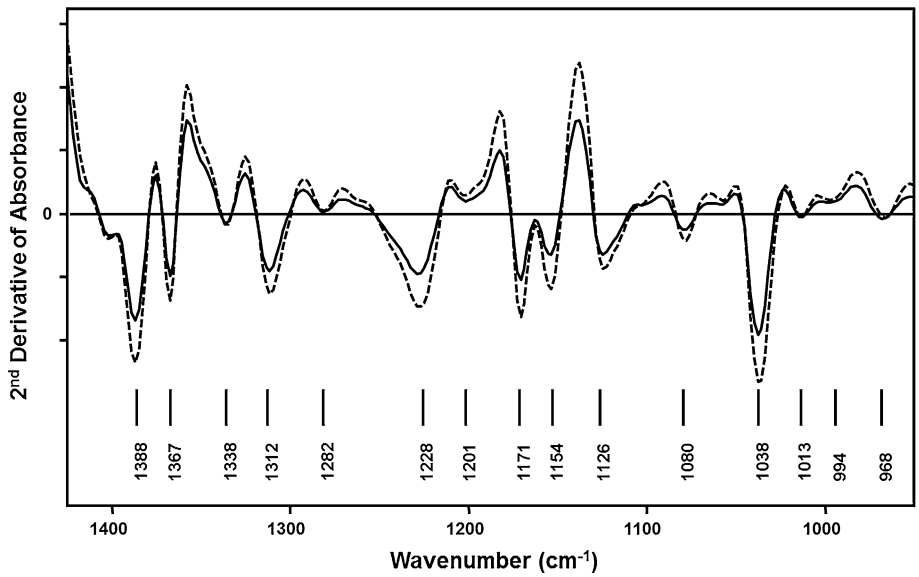

Fig. 3 NDP and LPD group average second derivative spectra for the data presented in Fig. 2

to have lower absorbance in carbohydrates. In contrast to the results found for lipids and for the "mixed" contribution band, the spatial distribution of carbohydrates did not closely follow the protein content in either the NPD or LPD offspring.

Discussion

The findings of this study have demonstrated, using FTIR micro-spectroscopy, that the biochemical composition of the LV myocardium is markedly altered in adult rats that were growth restricted in early life as a result of maternal protein restriction. There was a marked upregulation in the intensity of lipids, proteoglycans and carbohydrates in the LV myocardium of the LPD offspring; such dramatic changes in the biochemical composition of the myocardium are a potential cause of the abnormalities in cardiac function observed in adult life in growth-restricted offspring.

The greatest difference in the biochemical composition of the myocardium between the NPD and LPD offspring was observed in the "mixed" contribution band (1,228 cm^{-1}). The 1,228 cm^{-1} band arises from several contributing functional groups (Table 1) such as: (a) the protein amide III mode, (b) the asymmetric phosphate stretching vibration from nucleic acids, phospholipids and phosphorylated proteins and (c) the sulfate symmetric stretch from proteoglycans. Undoubtedly, all these macromolecules are present in

the LV free wall; however, it appears that they are not all responsible for the change in absorbance in this band between the two groups. It is tempting to ascribe the change in absorbance in the mixed contributions band as due to an increased collagen fraction of the total protein in the LPD offspring heart tissue compared to the controls. Elevated collagen expression has been previously observed by FTIR micro-spectroscopy in cardiomyopathic hearts from hamsters [18]. Spectral markers characteristic for collagen include four bands found at 1,338, 1,284, 1,240 and 1,204 cm^{-1} [18]. All of these bands are present in the spectra for the LPD and NPD offspring heart tissue indicating the presence of collagen. However, the three bands at 1,338, 1,284 and 1,204 cm^{-1} are unchanged between the two groups in the second derivative spectra (Fig. 3) indicating no discernable increase in collagen content in the LV free wall of LPD offspring compared to controls. We then confirmed this by assessing collagen content using image analysis of picrosirius red-stained LV tissue; there was no difference in the levels of interstitial collagen between the LPD and NPD group. This is in contrast to our previous findings of increased fibrosis in LPD female rats [21]; however, those rats were examined at an older age (24 weeks of age); hence, there may be a differential increase in collagen deposition with advancing age [30]. In the present study, although we found no differences in total collagen between the groups, it is possible that there may be differences in the proportion of the collagen subtypes, in particular collagens types I and III. Indeed, it is the change in the ratio of type I to type III collagen that is considered important in diseased hearts rather than the total amount of fibrosis [16, 31]. Currently, it remains difficult to detect the different collagen subtypes by FTIR micro-spectroscopy. Belbachir et al. have described this and succeeded but only for pure type samples [32].

Within the "mixed" contribution band, the spectral analysis also clearly demonstrated that there was no

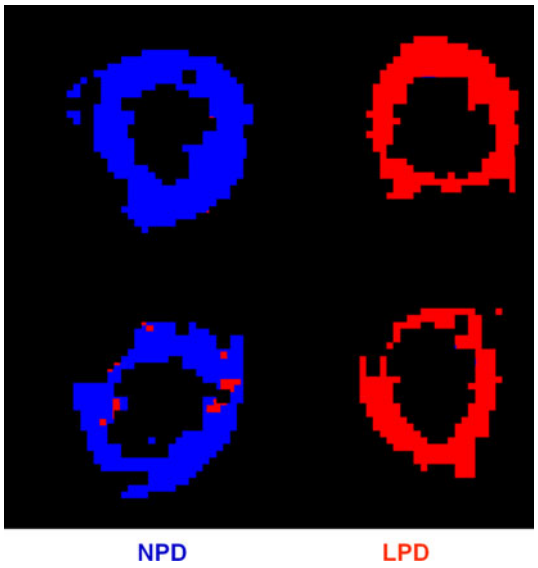

Fig. 4 UHC analysis maps of whole LV tissue sections, based on spectra in the range 1,800–950 cm^{-1}. UHC analysis separated the collected spectra into two groups (*red* and *blue*) based on spectral similarity. The appearance of the NPD samples (*left*) in mostly *blue* and the LPD samples (*right*) in *red* indicates that UHC analysis has readily distinguished the two groups as having spectra that are statistically different from each other. Only a small number of spectra have been misclassified (*red* pixels in the NPD sections)

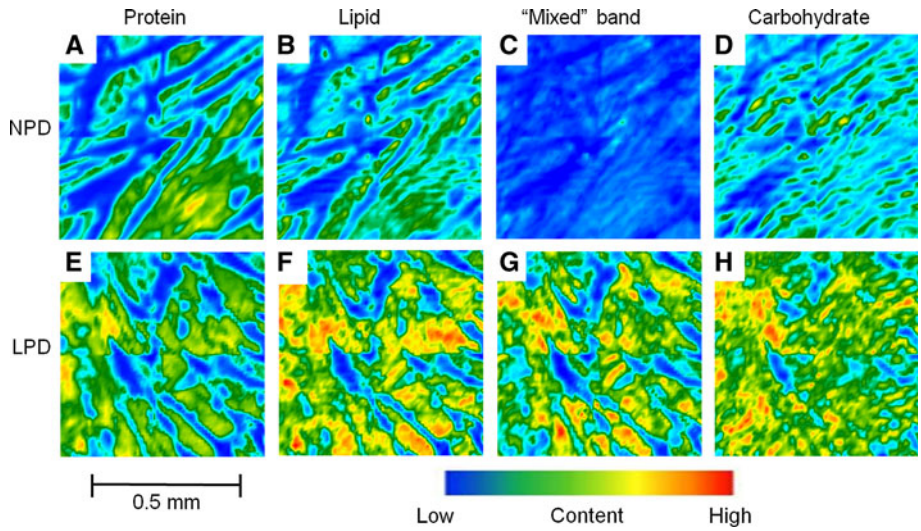

Fig. 5 LV free wall chemical images, based on the integrated areas indicated in Fig. 1, for proteins, lipids, the "mixed" contributions band and carbohydrates in the NPD and LPD groups. Images **a–d** represent a typical LV free wall tissue section from the NPD group; images **e–h** represent the LPD group. Warmer (*red*) colors represent areas of higher absorbance and the cooler (*blue*) colors represent regions of least absorbance. The tissues have undergone shrinkage during the processing, hence in the visible light micrographs open spaces appeared that showed no absorbance and thus appeared as the *darkest blue* color in the FTIR images

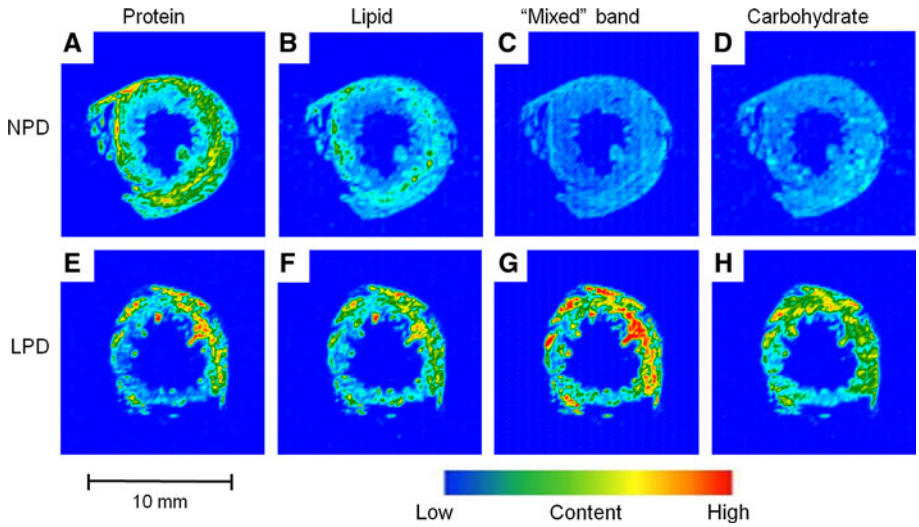

Fig. 6 Whole LV tissue sections including adjoining interventricular septum and papillary muscles chemical images, based on the integrated areas indicated in Fig. 1, for proteins, lipids, the "mixed" contributions band and carbohydrates in the NPD and LPD groups. Images **a–d** represent a whole LV tissue section for the NPD group; images **e–h** represent the LPD group for the same hearts presented in Fig. 5. Warmer (*red*) colors represent areas of higher absorbance and the cooler (*blue*) colors represent regions of least absorbance

detectable change in nucleic acids, and hence, the observed increase in the "mixed" contribution band at 1,228 cm^{-1} is likely due to changes in proteoglycans. Normal cardiac tissue produces several distinct proteoglycans; they are found in the basement membrane, cell surface and interstitial extra cellular matrix. Their synthesis, secretion, organization and degradation are complex and tightly regulated processes influenced by physical and chemical factors [33]. An increase in proteoglycan deposition can ultimately affect cardiac performance and vascular compliance [33]. FTIR spectra of proteoglycans are characterized by 1,216–1,255 cm^{-1} (symmetric sulfate stretch) [34–37] and bands in the range 1,031–1,080 cm^{-1} [37, 38]. The sulfate stretch is pronounced in the spectra due to the prevalence of sulphation of the glycosaminoglycan chains in proteoglycans [10, 36]. In our study, all of the above-described proteoglycan bands were observed in the spectra of the LV myocardium and importantly, all of these bands were more pronounced and exhibited increased absorbance in the hearts of LPD offspring when compared to controls.

The spatial distribution of the increased proteoglycan content in the LPD offspring (Fig. 5g) showed a very similar spatial distribution to that seen for protein in the wall of the LV in the LPD offspring (Fig. 5e), indicating that the increased proteoglycans were associated with the proteins and deposited in similar regions of the myocardium as the proteins. Likewise, there was upregulation of lipids within the myocardium of the LPD offspring and their spatial distribution also followed that of the protein distribution. In contrast, the carbohydrate content that was also increased in the LPD myocardium did not resemble the spatial distribution of the proteins.

There is a large body of experimental evidence linking IUGR with the programming of impaired glucose metabolism, increased adiposity and metabolic syndrome in later life [39–43] thus supporting our findings, of increased lipid and carbohydrate deposition in the hearts of LPD offspring. Interestingly however, we have recently shown in this model of maternal protein restriction that there is improved insulin sensitivity and normal whole-body composition (using dual X-ray absorptiometry analysis) in adult offspring exposed to maternal protein restriction; we suggest that these effects likely relate to the persistent attenuation of growth postnatally such that growth in utero reflected growth after birth [44]. Of concern, however, although the overall whole-body composition appears to be normal, the results from the present study demonstrate abnormal deposition of lipids within the myocardium. Whether this is also the case in other organs is yet to be examined.

The increase in carbohydrates within the myocardium of the growth-restricted offspring is also an important finding of this study and again is indicative of altered glucose metabolism within the LPD offspring. When there is an excess of glucose, it is generally stored within tissues in the form of starch/glycogen and lipids [45].

The time point when the biochemical changes first developed within the myocardium of the growth-restricted offspring is at this stage unknown. Certainly, the biochemical changes that we have observed in the adult myocardium in our growth-restricted offspring may have developed in early life. In support of this idea, a previous study by Tappia et al. [46] has reported an altered phospholipid profile and fatty acid content within the heart of LPD offspring by the time of birth.

In conclusion, FTIR micro-spectroscopy clearly demonstrates an increase in lipids, carbohydrates and proteoglycans within the adult myocardium following early life growth restriction. These changes in the biochemical composition of the myocardium provide a likely mechanism for the increased vulnerability to cardiovascular disease later in life, in individuals that were born of low birth weight. Whether the observed biochemical changes in the

heart are specific to IUGR due to maternal protein restriction or are a generalized consequence to all forms of IUGR (for example, IUGR due to hypoxia) is yet to be elucidated.

Acknowledgments The authors thank to Mr. Ian Boundy for his advice with histological preparation of the tissue. V. Z., M. J. B., J. T. P., B. R. W. and K. R. B. designed the research, V. Z. bred and maintained the rats for these experiments, processed and sectioned the heart tissue and performed the experiments, V. Z. and K. R. B. analyzed the data, B. R. W. interpreted micro-spectroscopy results, V. Z., M. J. B., J. T. P., K. R. B. wrote the paper. This study was supported by an Australian Postgraduate Research Award to V. Z. and Australian Research Council Discovery Grant to B. R. W.

References

1. Beargie RA, James VL Jr, Greene JW Jr (1970) Growth and development of small-for-date newborns. Pediatr Clin N Am 17(1):159–167
2. Camm EJ, Hansell JA, Kane AD, Herrera EA, Lewis C, Wong S, Morrell NW, Giussani DA (2010) Partial contributions of developmental hypoxia and undernutrition to prenatal alterations in somatic growth and cardiovascular structure and function. Am J Obstet Gynecol 203(5):495e24–495e34
3. Langley-Evans SC (2009) Nutritional programming of disease: unravelling the mechanism. J Anat 215(1):36–51
4. Langley-Evans SC, McMullen S (2010) Developmental origins of adult disease. Med Princ Pract 19(2):87–98
5. Meyer K, Lubo Z (2007) Fetal programming of cardiac function and disease. Reprod Sci 14(3):209–216
6. Barker DJ, Winter PD, Osmond C, Margetts B, Simmonds SJ (1989) Weight in infancy and death from ischaemic heart disease. Lancet 2(8663):577–580
7. Kaijser M, Bonamy AK, Akre O, Cnattingius S, Granath F, Norman M, Ekbom A (2008) Perinatal risk factors for ischemic heart disease: disentangling the roles of birth weight and preterm birth. Circulation 117(3):405–410
8. Rich-Edwards JW, Stampfer MJ, Manson JE, Rosner B, Hankinson SE, Colditz GA, Hennekens CH, Willet WC (1997) Birthweight and risk of cardiovascular disease in a cohort of women followed up since 1976. BMJ 315:396–400
9. Crispi F, Bijnens B, Figueras F, Bartrons J, Eixarch E, Le Noble F, Ahmed A, Gratacos E (2010) Fetal growth restriction results in remodeled and less efficient hearts in children. Circulation 121(22):2427–2436
10. Khorram O, Momeni M, Desai M, Ross MG (2007) Nutrient restriction in utero induces remodeling of the vascular extracellular matrix in rat offspring. Reprod Sci 14(1):73–80
11. Li G, Xiao Y, Estrella JL, Ducsay CA, Gilbert RD, Zhang L (2003) Effect of fetal hypoxia on heart susceptibility to ischemia and reperfusion injury in the adult rat. J Soc Gynecol Investig 10(5):265–274
12. Xu Y, Williams SJ, O'Brian D, Davidge ST (2006) Hypoxia or nutrients restriction during pregnancy in rats leads to progressive cardiac remodeling and impairs postischemic recovery in adult male offspring. FASEB J 20:E536–E545
13. Cheema KK, Dent MR, Saini HK, Aroutiounova N, Tappia PS (2005) Prenatal exposure to maternal undernutrition induces adult cardiac dysfunction. Br J Nutr 93(4):471–477
14. Tappia PS, Guzman C, Dunn L, Aroutiounova N (2011) Adverse cardiac remodeling due to maternal low protein diet is associated with alterations in expression of genes regulating glucose metabolism. Nutr Metab Cardiovasc Dis [Epub ahead of print]
15. Borg TK, Rubin K, Carver W, Samarel AT, Terracio L (1996) The cell biology of the cardiac interstitium. Trends Cardiovas Med 6:65–70
16. Hein S, Schaper J (2001) The extracellular matrix in normal and diseased myocardium. J Nucl Cardiol 8(2):188–196
17. McNaughton D, Wood B, Cox T, Drenckhahn J, Bambery K (2009) 3-D imaging of biomedical samples. In: Salzer R, Siesler HW (eds) Infrared and Raman spectroscopic imaging. Wiley, Weinheim, pp 203–221
18. Gough KM, Zelinski D, Wiens R, Rak M, Dixon IM (2003) Fourier transform infrared evaluation of microscopic scarring in the cardiomyopathic heart: effect of chronic AT1 suppression. Anal Biochem 316(2):232–242
19. Liu K, Jackson M, Sowa MG, Ju H, Dixon IM, Mantsch HH (1996) Modification of the extracellular matrix following myocardial infarction monitored by FTIR spectroscopy. Biochim Biophys Acta 1315(2):73–77
20. Severcan F, Toyran N, Kaptan N, Turan B (2000) Fourier transform infrared study of the effect of diabetes on rat liver and heart tissues in the CH region. Talanta 53(1):55–59
21. Lim K, Zimanyi MA, Black MJ (2006) Effect of maternal protein restriction in rats on cardiac fibrosis and capillarization in adulthood. Pediatr Res 60(1):83–87
22. Zohdi V, Jane Black M, Pearson JT (2011) Elevated vascular resistance and afterload reduce the cardiac output response to dobutamine in early growth-restricted rats in adulthood. Br J Nutr 106:1374–1382
23. Zimanyi MA, Bertram JF, Black MJ (2004) Does a nephron deficit in rats predispose to salt-sensitive hypertension? Kidney Blood Press Res 27(4):239–247
24. Gundersen HJ, Jensen EB, Kieu K, Nielsen J (1999) The efficiency of systematic sampling in stereology—reconsidered. J Microsc 193(Pt 3):199–211
25. Bambery KR, Wood BR, Quinn MA, McNaughton D (2004) Fourier transform infrared imaging and unsupervised clustering applied to cervical biopsies. Aust J Chem 57:1139–1143
26. Bassan P, Byrne HJ, Bonnier F, Lee J, Dumas P, Gardner P (2009) Resonant Mie scattering in infrared spectroscopy of biological materials—understanding the 'dispersion artefact'. Analyst 134(8):1586–1593
27. Jackson M, Choo LP, Watson PH, Halliday WC, Mantsch HH (1995) Beware of connective tissue proteins: assignment and implications of collagen absorptions in infrared spectra of human tissues. Biochim Biophys Acta 1270(1):1–6
28. Toyran N, Lasch P, Naumann D, Turan B, Severcan F (2006) Early alterations in myocardia and vessels of the diabetic rat heart: an FTIR microspectroscopic study. Biochem J 397(3):427–436
29. Romeo MJ, Diem M (2005) Infrared spectral imaging of lymph nodes: strategies for analysis and artifact reduction. Vib Spectrosc 38(1–2):115–119
30. Cornwell GG 3rd, Thomas BP, Snyder DL (1991) Myocardial fibrosis in aging germ-free and conventional Lobund-Wistar rats: the protective effect of diet restriction. J Gerontol 46(5):B167–B170
31. Norton GR, Tsotetsi J, Trifunovic B, Hartford C, Candy GP, Woodiwiss AJ (1997) Myocardial stiffness is attributed to alterations in cross-linked collagen rather than total collagen or phenotypes in spontaneously hypertensive rats. Circulation 96(6):1991–1998
32. Belbachir K, Noreen R, Gouspillou G, Petibois C (2009) Collagen types analysis and differentiation by FTIR spectroscopy. Anal Bioanal Chem 395(3):829–837
33. Wight TN (1989) Cell biology of arterial proteoglycans. Arteriosclerosis 9(1):1–20

34. Camacho NP, West P, Torzilli PA, Mendelsohn R (2001) FTIR microscopic imaging of collagen and proteoglycan in bovine cartilage. Biopolymers 62(1):1–8
35. Crombie DE, Turer M, Zuasti BB, Wood B, McNaughton D, Nandakumar KS, Holmdahl R, Van Damme MP, Rowley MJ (2005) Destructive effects of murine arthritogenic antibodies to type II collagen on cartilage explants in vitro. Arthritis Res Ther 7(5):R927–R937
36. Garnjanagoonchorn W, Wongekalak L, Engkagul A (2007) Determination of chondroitin sulfate from different sources of cartilage. Chem Eng Process 46:465–471
37. Potter K, Kidder LH, Levin IW, Lewis EN, Spencer RG (2001) Imaging of collagen and proteoglycan in cartilage sections using Fourier transform infrared spectral imaging. Arthritis Rheum 44(4):846–855
38. Ben Mansour M, Dhahri M, Bertholon I, Ollivier V, Bataille I, Ajzenberg N, Hassine M, Jandrot-Perrus M, Chaubet F, Maaroufi RM (2009) Characterization of a novel dermatan sulfate with high antithrombin activity from ray skin (*Raja radula*). Thromb Res 123(6):887–894
39. Fagundes AT, Moura EG, Passos MC, Santos-Silva AP, de Oliveira E, Trevenzoli IH, Casimiro-Lopes G, Nogueira-Neto JF, Lisboa PC (2009) Temporal evaluation of body composition, glucose homeostasis and lipid profile of male rats programmed by maternal protein restriction during lactation. Horm Metab Res 41(12):866–873
40. Herrera E, Lopez-Soldado I, Limones M, Amusquivar E, Ramos MP (2005) Experimental models for studying perinatal lipid metabolism. Long-term effects of perinatal undernutrition. Adv Exp Med Biol 569:95–108
41. Ozanne SE, Hales CN (2002) Early programming of glucose-insulin metabolism. Trends Endocrinol Metab 13(9):368–373
42. Petry CJ, Hales CN (2000) Long-term effects on offspring of intrauterine exposure to deficits in nutrition. Hum Reprod Update 6(6):578–586
43. Zambrano E, Bautista CJ, Deas M, Martinez-Samayoa PM, Gonzalez-Zamorano M, Ledesma H, Morales J, Larrea F, Nathanielsz PW (2006) A low maternal protein diet during pregnancy and lactation has sex- and window of exposure-specific effects on offspring growth and food intake, glucose metabolism and serum leptin in the rat. J Physiol 571(Pt 1):221–230
44. Lim K, Armitage JA, Stefanidis A, Oldfield BJ, Black MJ (2011) Intrauterine growth restriction in the absence of postnatal 'catch-up' growth leads to improved whole body insulin sensitivity in rat offspring. Pediatr Res 70:339–344
45. Nelson DL, Cox MM (eds) (2000) Biosynthesis of glycogen, starch, sucrose and other carbohydrates. In: Lehninger principles of biochemistry. Worth Publishers, New York, pp 722–744
46. Tappia PS, Nijjar MS, Mahay A, Aroutiounova N, Dhalla NS (2005) Phospholipid profile of developing heart of rats exposed to low-protein diet in pregnancy. Am J Physiol Regul Integr Comp Physiol 289(5):R1400–R1406
47. Toyran N, Turan B, Severcan F (2007) Selenium alters the lipid content and protein profile of rat heart: an FTIR microspectroscopic study. Arch Biochem Biophys 458(2):184–193
48. Cakmak G, Togan I, Uguz C, Severcan F (2003) FT-IR spectroscopic analysis of rainbow trout liver exposed to nonylphenol. Appl Spectrosc 57(7):835–841
49. Wood BR, Quinn MA, Burden FR, McNaughton D (1996) An investigation intio FTIR spectroscopy as a biodiagnostic tool for cervical cancer. Biospectroscopy 2(3):143–153
50. Lyman DJ, Murray-Wijelath J (1999) Vascular graft healing: I. FTIR analysis of an implant model for studying the healing of a vascular graft. J Biomed Mater Res 48(2):172–186
51. Banyay M, Sarkar M, Graslund A (2003) A library of IR bands of nucleic acids in solution. Biophys Chem 104(2):477–488